Journal of Biomedical Optics

BiomedicalOptics.SPIEDigitalLibrary.org

Combined Raman and autofluorescence *ex vivo* diagnostics of skin cancer in near-infrared and visible regions

Ivan A. Bratchenko
Dmitry N. Artemyev
Oleg O. Myakinin
Yulia A. Khristoforova
Alexander A. Moryatov
Sergey V. Kozlov
Valery P. Zakharov

SPIE.

Ivan A. Bratchenko, Dmitry N. Artemyev, Oleg O. Myakinin, Yulia A. Khristoforova, Alexander A. Moryatov, Sergey V. Kozlov, Valery P. Zakharov, "Combined Raman and autofluorescence *ex vivo* diagnostics of skin cancer in near-infrared and visible regions," *J. Biomed. Opt.* **22**(2), 027005 (2017), doi: 10.1117/1.JBO.22.2.027005.

Combined Raman and autofluorescence *ex vivo* diagnostics of skin cancer in near-infrared and visible regions

Ivan A. Bratchenko,[a,*] Dmitry N. Artemyev,[a] Oleg O. Myakinin,[a] Yulia A. Khristoforova,[a] Alexander A. Moryatov,[b] Sergey V. Kozlov,[b] and Valery P. Zakharov[a]
[a]Samara National Research University, Department of Laser and Biotechnical Systems, Samara, Russia
[b]Samara State Medical University, Department of Oncology, Samara, Russia

Abstract. The differentiation of skin melanomas and basal cell carcinomas (BCCs) was demonstrated based on combined analysis of Raman and autofluorescence spectra stimulated by visible and NIR lasers. It was *ex vivo* tested on 39 melanomas and 40 BCCs. Six spectroscopic criteria utilizing information about alteration of melanin, porphyrins, flavins, lipids, and collagen content in tumor with a comparison to healthy skin were proposed. The measured correlation between the proposed criteria makes it possible to define weakly correlated criteria groups for discriminant analysis and principal components analysis application. It was shown that the accuracy of cancerous tissues classification reaches 97.3% for a combined 6-criteria multimodal algorithm, while the accuracy determined separately for each modality does not exceed 79%. The combined 6-D method is a rapid and reliable tool for malignant skin detection and classification. [DOI: 10.1117/1.JBO.22.2.027005]

Keywords: Raman spectroscopy; autofluorescence; principal component analysis–discriminant analysis; optical diagnostics; oncology; melanoma; basal cell carcinoma.

Paper 160696PR received Oct. 13, 2016; accepted for publication Jan. 31, 2017; published online Feb. 16, 2017.

1 Introduction

The problem of increased incidence of cancer is known worldwide. For example, more than 550 thousand cases of cancer are registered yearly in Russia and about 13% to 15% of all deaths are caused by cancer.[1] The predominant forms of cancer in Russia are cancers of digestive organs and peritoneum (37.2%), lung and bronchus cancers for men (30.2%), and breast cancer for women (17.1%).[2] One of the most dangerous cancers is malignant melanoma (MM) as it causes more than 76% deaths among all skin cancers. Lack of timely medical care, weak efficiency of first-hand clinical examinations, and aging of the population provoke rising cancer incidence and cancer mortality rates.[1,2] In this regard, it is necessary to find effective and fast methods of early cancer detection and classification.

In recent decades, a number of optical methods have been used for cancer detection and imaging, including confocal microscopy,[3] optical coherence tomography (OCT),[4] and multiphoton tomography (MPT).[5] For example, MPT in combination with fluorescence lifetime imaging (FLIM) may provide label-free imaging with subcellular resolution and thereby significantly increase overall accuracy of tumor diagnostics—a sensitivity of 100% and a specificity of 98% were reached for the diagnosis of MM.[6] MPT/FLIM can be performed using fast detection electronics and complicated equipment, which make it hard to explore difficult body sites or irregular surfaces.[7] The depth of the focus plane in the tissue reaches levels of 200 μm. Thus, only the superficial part of skin tumors can be studied by MPT. OCT may extend the depth of visualization up to 1 to 2 mm, which in most cases is enough for basal cell carcinomas (BCC) determination due to unique BCC space structure.[8] Also OCT images of oncological pathologies were tested using color, fractal, and texture features,[9] but the possibility of tumor diagnosis with these features is still under consideration[10] as malignant and premalignant tumors do not have distinctive patterns in OCT images.[11]

Tumor diagnosis is possible with spectroscopy techniques, such as elastic scattering,[12] Raman spectroscopy (RS),[13] autofluorescence (AF)[14] analysis, and Stokes shift spectroscopy.[15] RS wavelength shift and intensity of inelastic scattering caused by interaction of light with different vibration types of tissue components were used for tumor classification in numerous investigations due to today's breakthroughs in detecting weak signals. For example, the diagnostic accuracy of RS study of gastric[16] and skin[13] pathologies is as high as 90% to 96% and 80% to 95%, respectively. AF tumor studies in general show lower accuracy in comparison with RS,[17] but AF is characterized by much higher intensity which makes it possible to register signals within a short period of time and rapidly scan the tumor area. Thus, there is a need in clinical trials to optimize AF efficiency and validity for cancer diagnostics.[18]

Many authors[19,20] have noted the decrease in the efficiency of cancer detection in clinical trials with large numbers of tested samples due to great variability of sample features and their chemical components. This effect may be partly compensated (approximately by 5% to 10%) in a multimodal approach,[21] when each modality uses optical parameters associated with different tissue components altering during the cancerous process. The combination of RS and AF has been demonstrated for

*Address all correspondence to: Ivan A. Bratchenko, E-mail: iabratchenko@gmail.com

1083-3668/2017/$25.00

gastric,[21] lung,[22,23] liver,[24] and breast tissues model[25] experiments. Yet the exact RS–AF diagnostic accuracy is still unclear for different skin tumor types. We may also improve the diagnostic accuracy by comparing the composition of the main tissue chromophores in the tumor area and the normal skin of the same patient.[26] Such "normal tissue" contrast helps to avoid the influence of individual skin properties and the inherent heterogeneity of the tissue on experimental results.

The aim of this study is to develop a set of highly sensitive methods to analyze specific skin tissue components and to design a complex method of MM and BCC diagnosis involving the combination of RS and AF. Such an approach helps to determine and compare the accuracy of malignant tumors classification for each of the proposed methods and for any of their combinations. The advantage of a complex method lies in enhancing tumor determination accuracy as each method is based on alteration of different reference tissue components. While RS helps to monitor changes related to collagens, other proteins, and lipids, a near-infrared (NIR) AF study reveals changes in concentration of melanin, visible (VIS) AF helps to estimate changes in content of porphyrins, flavins, and lipids.

2 Materials and Methods

2.1 *Experimental Setup and Spectra Acquisition*

The laboratory setup is presented in Fig. 1; it combines principles of RS and AF for human skin tissue studies. The setup includes a thermally stabilized semiconductor NIR diode laser module LML-785.0RB-04 (785 ± 0.1 nm central wavelength, 150 mW) for excitation of Raman spectra and AF in the NIR region and a diode-pumped solid-state laser module (457 nm, 200 mW) for AF stimulation in the visible region. Laser radiation is delivered to the optical detector by excitation fibers (100 μm diameter, 0.22 NA) and collimating lenses L_1 and L_2. NIR (785 nm) laser radiation passes through the bandpass filter (BPF), which cuts off the Raman component of the optical fiber. The first (DM_1) and second (DM_2) dichroic mirrors transmit 785- and 457-nm laser radiation to lens L_3, which focuses exciting radiation onto the sample (7.5-mm focal length). The same lens L_3 collects RS, AF, and backscattered radiation. Dichroic mirror DM_3 splits collected radiation on VIS and NIR channels, which include an appropriate longpass filter (LPF_1/LPF_2) to cut off exciting (NIR/VIS) laser radiation, matching lens (L_4/L_5), and collection fibers (200 μm diameter, 0.22 NA), connected to multichannel spectrograph Shamrock SR-500i-D1-R with an Andor iDus CCD digital camera DU416A-LDC-DD cooled up to −65°C. The experimental setup was calibrated consequentially for RS and both NIR and VIS AF signals. Low-noise recording of RS and AF radiation was performed in spectral bands 790 to 930 nm and 560 to 750 nm with spectral resolution better than 0.05 nm.

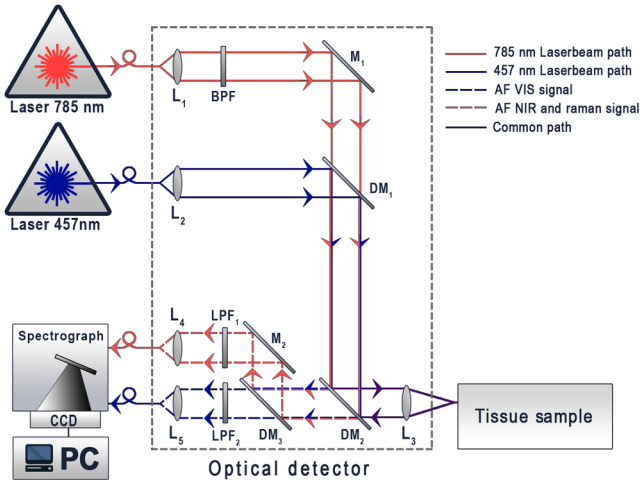

Fig. 1 Experimental setup: L_1, L_2, L_4, and L_5: matching lenses, L_3: focusing lens, BPF: bandpass filter, M_1 and M_2: mirrors, DM_1, DM_2, and DM_3: dichroic mirrors, and LPF_1 and LPF_2: longpass filters.

The optical detector was positioned directly over the tissue sample at a distance of 7 to 8 mm. The beam diameter of the probing radiation on the tissue was 1.5 mm. Measurement depth was about 1 to 2 mm. The laser power on the skin was 30 mW for both lasers, which corresponds to the laser density 1.7 W/cm^2 on the skin. The acquisition time was 15 s for VIS AF and 30 s for RS and NIR AF analysis.

All tissue samples were irradiated by NIR laser during 2 to 3 min before spectra registration in order to increase RS signal-to-noise ratio due to decreasing NIR AF intensity by the effect of tissues photobleaching while the intensity of Raman scattering remains unchanged.[27] It is important to note that the shape of the AF spectral function remains the same during 2 to 3 min of the photobleaching process and only NIR AF intensity monotonically decreases. This monotonic decrease of AF spectra during the photobleaching process was also observed by Wang et al.[28]

NIR and VIS signals were registered consequently from the same tissue areas. Raman and AF spectra were acquired for a tumorous region and normal skin closely adjacent to a lesion (within 2 to 4 cm). Three independent spectra measurements were made for each predefined by medical personnel spatial point, and then an averaged value was calculated for mean spectrum. It helps to calculate the changes in malignant tissue in comparison with normal tissue and compose relative criteria (see Sec. 2.3), which exclude the influence of individual variability of skin properties on obtained results.

2.2 *Tissue Samples*

There were 79 patients with skin cancers (38 female and 41 male, all white, Caucasian, skin phenotype I and II) enrolled in this study. *Ex vivo* tissue samples were obtained after surgical resection at Samara Regional Clinical Oncology Dispensary under an approved protocol including patient agreement. The first cohort of 158 samples (79 healthy skins, 39 MM, and 40 BCC) underwent RS and NIR AF analysis. The second cohort of 74 samples (37 normal skins, 27 BCC, and 10 MM) underwent RS and AF spectra registration in visible and NIR regions. Tissue samples were stored in sterile boxes at $+4 \pm 2$°C and were tested using an experimental setup no later than 4 h after resection. The skin tumor samples were $\sim 2 \times 2 \times 1$ cm^3 in size. All samples were divided into two pieces containing both a healthy tissue region and part of the tumor. One sample piece underwent experimental tests. The rest of the sample was fixed in formalin and prepared for histological analysis. The detailed distribution of human skin lesions, including information about tumor locations, is provided in Table 1.

Every tumor study was accompanied by histological analysis to make a final diagnosis. The protocols of *ex vivo* tissue diagnostics were approved by the ethical committee of Samara State Medical University.

Table 1 Summary of skin tissue samples.

Subjects						Location		
Histology-approved diagnosis	Mean age, year (range)	Mean diameter, cm (range)	Male	Female	Number of lesions	Trunk	Upper limb	Lower limb
MM	60.5 (34 to 84)	1.68 (0.3 to 4)	17	22	39	21	8	10
BCC	70 (40 to 85)	2.11 (0.8 to 3.5)	24	16	40	23	13	4

2.3 *Spectra Processing and Data Analysis*

NIR laser radiation simultaneously stimulates Raman scattering and AF response in the NIR spectral range. The collected spectra contain a wide exponentially decaying AF spectra curve with sharp Raman peaks, which are usually separated by the method of AF polynomial approximation.[29] In the current study, this method was upgraded with additional filtering of random noises and automatic selection of polynomial order.

All processed RS, NIR AF, and VIS AF spectra may be grouped according to histological data and further statistically processed using principal component analysis (PCA) or other multivariate analysis techniques.[30] It is well known that the number of tested samples should be greater or of the same order as a number of variables for mathematically correct covariance decomposition. In addition, the entire RS/AF spectrum analysis may provide incomplete understanding of chemical changes responsible for disease diagnosis.[31] In this study, the analysis of obtained spectra was performed based on a number of *a priori* predefined spectral criteria described below. These criteria were associated with relative content of the main skin chromophores. Such an approach allowed for reduction in the number of variables from thousands (for the entire spectra) to a few variables and helps to include personal skin features in the analysis. It also helps us to register spectral information for understanding the differences between normal and cancerous tissues RS/AF spectra.

The RS analysis was performed with the help of a two-step phase-space analysis method,[26] which is based on alteration of ratio between RS spectral peaks I_k in the tumor area and the healthy tissue near the lesion. Normalized intensity I_k was defined as the ratio of maximum of RS intensity of k'th spectral band to the maximum RS intensity in the band 1440 to 1460 cm^{-1} as the most intensive RS band of typical Raman spectra for both cancer and normal skin (Fig. 2). Such an approach makes it possible to separate malignant and normal tissue in the first step. The differentiation of cancer types among selected cancerous samples was performed in the second step with the help of relative coefficients

$$\mathrm{RS}_k = \frac{|I_k^{(m)} - I_k^{(h)}|}{I_k^{(m)} + I_k^{(h)}}, \tag{1}$$

where $I_k^{(m)}$ and $I_k^{(h)}$ are absolute intensities of k'th spectral band for malignant (index m) and healthy (index h) skin tissues of the same sample. These coefficients utilize information from both tumor and normal skin near the lesion and, as a result, monitor the alteration of tumor chemical composition taking into account the individual characteristics of the patient's skin.

Coefficients [Eq. (1)] for the two most intensive spectral ranges $k = 1320$ and 1660 cm^{-1} form the phase plane which was used for tissue classification by discriminant analysis (DA). DA can separate two or more classes based on different statistical parameters of Gaussian distributions. The efficiency of the proposed approach is characterized by sensitivity and specificity and ability to select defined classes in different areas of phase plane. The analysis of skin tissues data allocation was performed using linear and quadratic DA classifiers.[32]

Within the spectral range 870 to 920 nm, NIR AF intensity decreases with the growth of the wavelength (Fig. 3), and the most significant qualitative changes of the NIR AF spectrum for different tumors were observed within the range of 810 to 870 nm. For the comparative analysis of the experimental data, we approximate the NIR AF spectrum with an exponential function

$$I_{\mathrm{ap}}(\lambda) = FI_{\mathrm{NIR}} * \exp^{F\lambda_{\mathrm{NIR}}\left(\frac{\lambda}{\lambda_{\max}}\right)} + c, \tag{2}$$

where the coefficient FI_{NIR} is responsible for the convex or concave behavior of the approximating function, the absolute value of the coefficient $F\lambda_{\mathrm{NIR}}$ characterizes the wavelength dependence curvature of AF spectra, and $\lambda_{\max} = 870$ nm is the right boundary of the approximation interval. The approximation was implemented using the criteria of minimizing the root-mean-square error with the Nelder–Mead simplex method and a stochastic method of differential evolution.[33] Details of AF spectra curvature calculation can be found elsewhere.[34]

According to observed VIS AF spectra (Fig. 4), we propose to use a number of criteria to monitor the changes of flavins, lipids, and porphyrins content in skin tissues. The most useful among them are the ratios between intensities of VIS AF spectra maxima in 570 to 590 nm (I_{570}) and 610 to 690 nm (I_{610}) ranges $FI_{\mathrm{VIS}} = \frac{I_{610}}{I_{570}}$ and normalized spectral maxima position shift

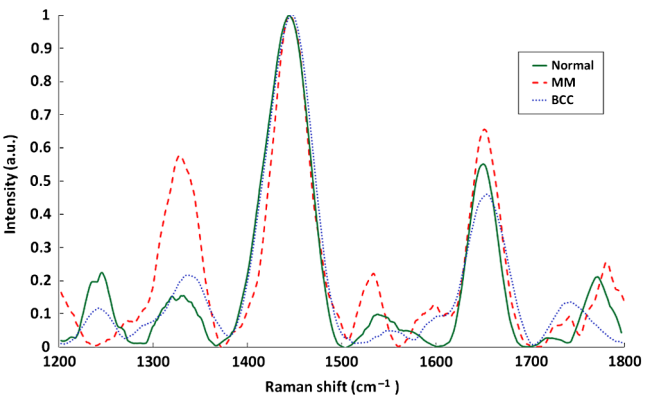

Fig. 2 Normalized *ex vivo* Raman spectra of normal skin tissue, MM, and BCC.

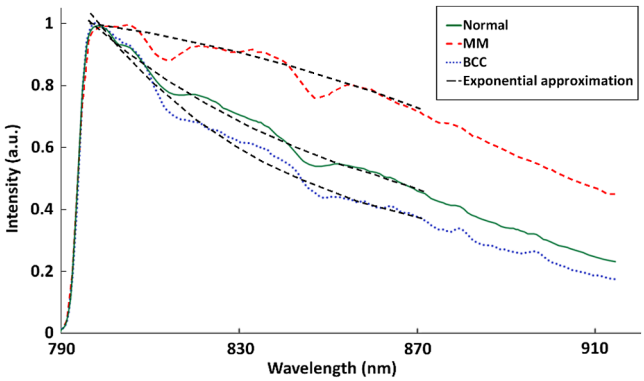

Fig. 3 Typical normalized *ex vivo* AF NIR spectra of normal skin, MM, and BCC.

$F\lambda_{\mathrm{VIS}} = \frac{|\lambda_{\mathrm{norm}}-\lambda_{\mathrm{tumor}}|}{\lambda_{\mathrm{norm}}+\lambda_{\mathrm{tumor}}}$, where λ_{tumor} and λ_{norm} are the position of AF maximum for tumor and normal skin near lesion for the same sample.[35] The value of FI_{VIS} is proportional to the relative concentration of total flavins and lipopigments content. VIS AF spectrum shift $F\lambda_{\mathrm{VIS}}$ helps to estimate changes in different types of porphyrins appearing on the upper skin layers, as tumors contain more bacteria on their surface than a normal skin which results in different porphyrins composition.

Such an approach makes it possible to define multidimensional space of different RS and AF criterial parameters. Each specific cancer type characterized by its own tissue components changes the equivalent to a specific set of criteria values. Thus, each cancer type fills in the exact area in multidimensional phase space, and, as a result, we have a mechanism for exact optical identification of tumor type. A correlation between the proposed criteria was estimated in order to find the groups of criteria with the lowest correlation for multidimensional space analysis. Pearson's correlation coefficients were calculated for each pair of proposed criteria.[36] Further analysis of multidimensional phase spaces based on chosen criteria was performed with PCA. This type of analysis helps to reduce the dimensionality of the data while retaining most of the variation in the data set. It uses directions, called principal components, along which the variation in the data is maximal. Isolating a number of components, each sample can be represented by relatively few numbers instead of multiple variables. Samples can then be plotted, making it possible to visually assess similarities and differences between samples.[37]

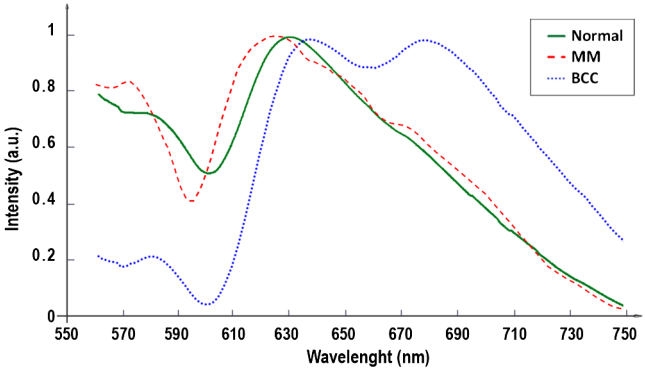

Fig. 4 Normalized VIS AF spectra of normal skin tissue, MM, and BCC stimulated by 457 nm laser.

3 Experimental Results

3.1 *Raman Spectroscopy Tissue Study*

Absolute values of RS intensity may differ significantly from one skin tissue sample to another due to high variability of tissue components concentration. Each spectrum was normalized to maximum intensity in the whole spectral range of 1200 to 1800 cm^{-1} in order to overcome this effect. Typical registered Raman spectra of MM, BCC, and healthy skin are presented in Fig. 2. The most intensive RS band of typical normalized Raman spectra[26] of cancer and normal skin is located at 1450 cm^{-1} and associated with CH_2 deformations of proteins and lipids. Other well observed bands are 1240 to 1280 cm^{-1} (stretching mode C═N), 1300 to 1340 cm^{-1} (twisting, wagging of bending mode CH_2), 1540 to 1580 cm^{-1} (deformation mode C═C and tryptophan), and 1640 to 1680 cm^{-1} (stretching mode C═O amide I).

The two-step RS analysis of skin samples is shown in Fig. 5. Here, every tested sample is a single point on the phase plane with coordinates corresponding to RS spectral coefficients of the two-step algorithm described in Sec. 2.3. Figure 5(a) represents the first step of analysis where we separate normal skin tissues from the malignant pathologies. Such classification is possible with a total accuracy 54.7% using linear DA. Accuracy of MM separation versus all other skin types reaches 72.7%. One may see that the areas of normal skin and BCC are mainly overlapping in Fig. 5(a) and thus the separation of malignant and normal skin tissue is complicated. Therefore, coefficients I_{1320} and I_{1660} were considered low informative for skin tissue analysis.

On the other hand, the problem of normal skin separation from malignant tissues is not so relevant in clinical practice as a problem of exact determination of malignant tissue type. It is more appropriate to separate MM from BCC. For this purpose, coefficients I_{1320} and I_{1660} were supplemented with coefficients RS_{1320} and RS_{1660}, which were used in the second step [Fig. 5(b)]. The overall accuracy of BCC and MM separation rose up to 80.3% for the two-step method.

The achieved accuracy is 8% lower than the accuracy shown in our previous study.[26] The decrease in accuracy is caused by larger dispersion of tissue components content due to threefold increase in the number of tested samples.

3.2 *Near-Infrared Autofluorescence Tissue Study*

As RS two-step analysis reveals the relative alteration of content of proteins and lipids in the tumor, the diagnostics accuracy may be improved by additional analysis of other tissue components. The melanin content proves to be a helpful additional criterion as MM are usually more pigmented lesions than BCC. Moreover, the content of pheomelanin and eumelanin may differ in malignant skin tumors.[38] Thus, measuring the melanin content may improve MM and BCC classification with optical methods.

Figure 3 demonstrates typical NIR AF spectra of normal skin and tumor stimulated by 785 nm laser. The dotted curve shows the exponential approximation [Eq. (2)] of NIR AF spectra. As the curvature (absolute value and its sign) and slope of approximation function depend on melanin content in the skin tissue, coefficients FI_{NIR} and $F\lambda_{\mathrm{NIR}}$ may be used for estimation of melanin value. And these coefficients may be measured simultaneously with Raman signal. Such an approach was first described in our study,[34] where only the curvature sign of the

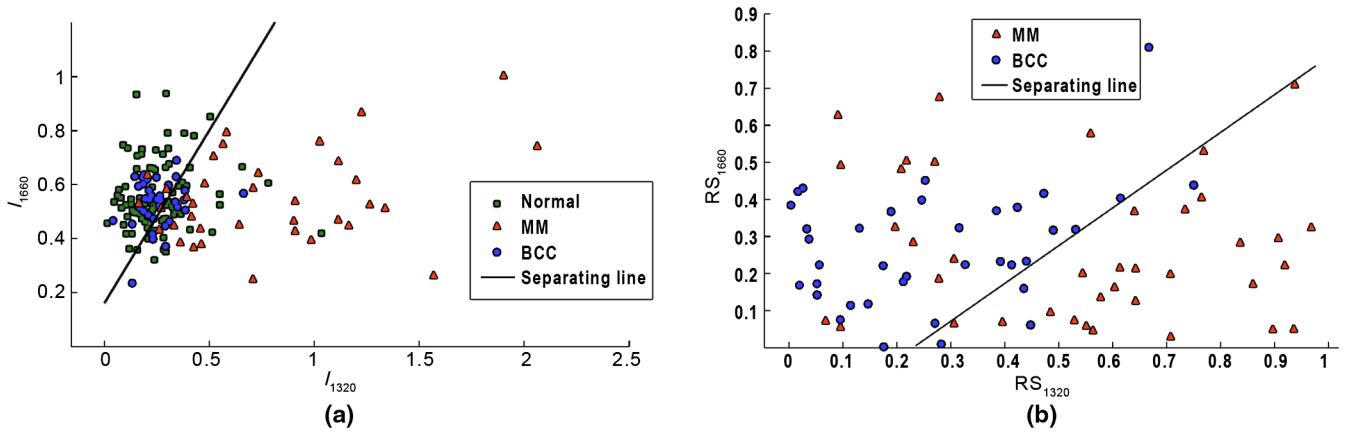

Fig. 5 Skin tissues classification by two-step RS algorithm: (a) the first step—MM versus all other skin tissues and (b) the second step—MM versus BCC.

spectrum approximation function [Eq. (2)] was used for sample differentiation. In the current study, we additionally use absolute values of the curvature (criterion FI_{NIR}) for MM and BCC separation. In general, analysis of coefficient FI_{NIR} showed a possibility to separate MM and BCC with a total accuracy of 60.8%.

The box-and-whisker plot (Fig. 6) demonstrates the values of coefficient $F\lambda_{\mathrm{NIR}}$ for MM, BCC, and normal skin classification. Note that median, first quartile, and minimum of $F\lambda_{\mathrm{NIR}}$ for BCC and normal skin have almost identical values. In the current study, it was assumed that the criterial norm $F\lambda_{\mathrm{NIR}} \geq 1$ for the maximum efficiency of MM selection among BCC and normal skin. The sensitivity and specificity for MM selection reached 69.2% and 85.0%, respectively, for this criterial norm.

Further increase in accuracy of malignant tumor detection with NIR AF may be achieved by combined analysis of both criteria (FI_{NIR} and $F\lambda_{\mathrm{NIR}}$): the result was considered positive when one of the criteria showed that the neoplasm is MM. In this case, the sensitivity of MM detection reaches 92.3%, but the overall accuracy of MM and BCC separation was only 64.6%.

3.3 *VIS Autofluorescence Tissue Study*

Unlike RS and NIR AF, the analysis of AF spectra stimulated in the visible region helps to reveal properties of lipids, flavins, and

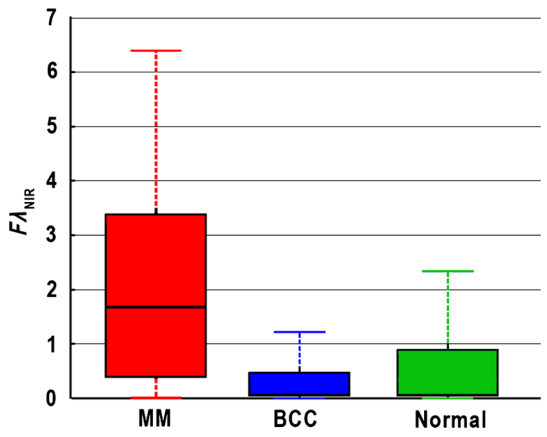

Fig. 6 Classification of MM, BCC, and normal skin based on melanin content (curvature $F\lambda_{\mathrm{NIR}}$ of registered AF spectra stimulated by 785 nm laser).

porphyrins in skin tissue. Skin lipids contribute to normal barrier function. Some lipids found on the skin's surface make the skin unfriendly to fungi and bacteria.[39] Porphyrins play a significant role in metabolism processes, including metabolism of bacteria on the skin surface.[40,41] Flavins control photostimulated generation of melanin within the specialized cells.[42] Thus, the synthesis of melanin in normal skin and tumors is related to the flavins present. Also, tumors are characterized by increased rate of metabolism processes and growing of MM or BCC causes the alteration of flavin and porphyrin concentrations, which are expressed in tumor color alteration in comparison with normal skin.

Typical VIS AF spectra have a local maximum in 570 to 590 nm for all skin types and maximum in spectral range of 610 to 690 nm (Fig. 4), which is a combination of two local maxima in 610 to 640 nm and 650 to 690 nm. Here, normal skin and MM have only one maximum in 629 and 623 nm, respectively, while BCC has two strong maxima of comparable intensity in 635 and 678 nm. Shown examples of spectra are common for studied skin tissues, but exact maxima positions and intensities may slightly differ from sample to sample. Redistribution of AF intensity between local maxima 610 to 640 nm and 650 to 690 nm is caused by changes in concentration of flavins and porphyrins and leads to the main maximum position shift. These changes may be defined by the spectral criteria pair FI_{VIS} and $F\lambda_{\mathrm{VIS}}$.

The possibility of MM and BCC separation by each VIS AF criteria is shown in Fig. 7. The sensitivity of MM detection equals 100% achieved for intensity threshold $FI_{\mathrm{VIS}} > 0.91$ or for spectral shift $F\lambda_{\mathrm{VIS}}$ between 1 and 19 nm. But the accuracy of such detection does not exceed 51%. One may see insufficient accuracy of MM detection based on single VIS AF criterion analysis. The increase in accuracy up to 75% may be achieved by simultaneous monitoring of both criteria as it is shown in Fig. 8. Here, classification of MM and BCC was performed with linear DA on phase plane of porphyrins composition on tissue surface ($F\lambda_{\mathrm{VIS}}$) and relative content of porphyrins, lipids, and flavins (FI_{VIS}).

3.4 *Combined Raman Spectroscopy–Autofluorescence Study*

As each proposed criterion refers to changes of different tumor components the enhancement of the classification accuracy may

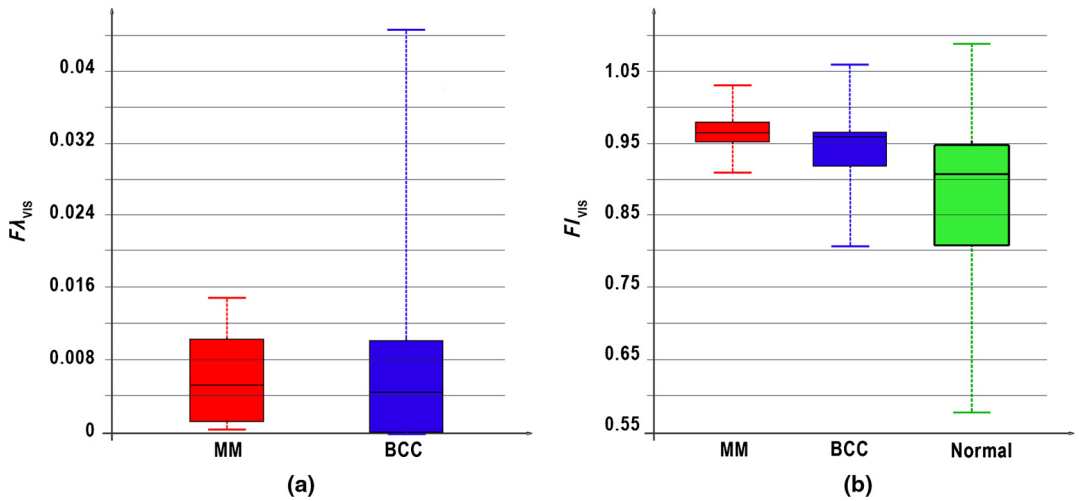

Fig. 7 Skin tissues classification based on VIS AF criteria: (a) porphyrins composition on tissue surface ($F\lambda_{VIS}$) and (b) relative content of porphyrins, lipids, and flavins (FI_{VIS}).

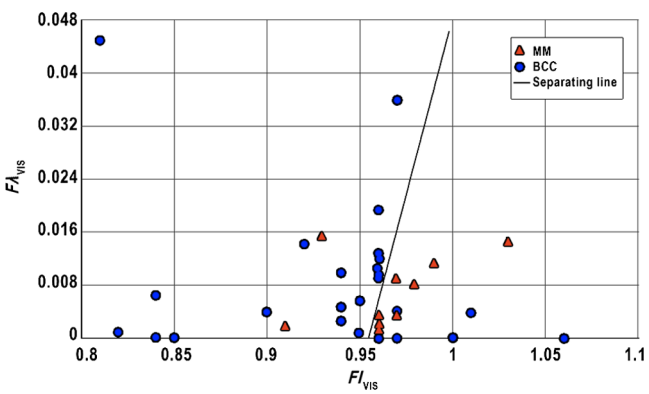

Fig. 8 MM and BCC classification on the phase plane with joint VIS AF monitoring of porphyrins composition ($F\lambda_{VIS}$) and relative content of porphyrins, lipids, and flavins (FI_{VIS}).

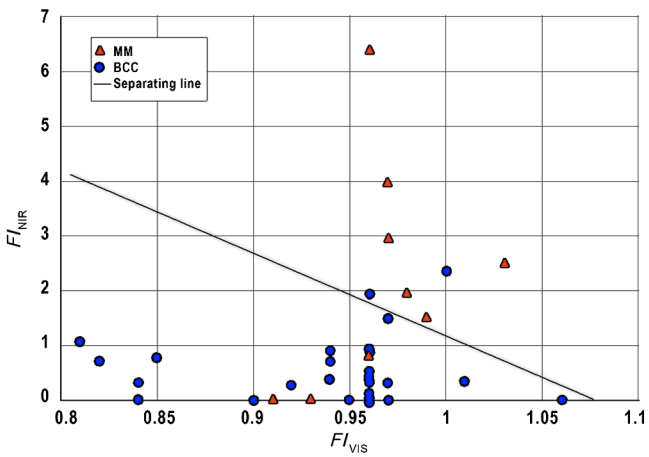

Fig. 9 MM and BCC classification on the phase plane with criteria FI_{VIS} and $F\lambda_{NIR}$.

be achieved by combination of criteria from different spectroscopic techniques. For instance, Fig. 9 contains the phase plane for analysis of criteria pair for relative porphyrins, lipids, and flavins content monitoring and melanin level estimation (FI_{VIS} and $F\lambda_{NIR}$). The combination of AF criteria in VIS and NIR regions provides 8% to 10% more accurate separation of MM and BCC in comparison with single NIR or VIS AF analysis.

Instead of using separate criteria pairs, it is more efficient to simultaneously analyze as many criteria as possible, i.e., using the information about all chosen tissue components in a multidimensional criteria space. Such classification was performed in 4-D space (FI_{NIR} and $F\lambda_{NIR}$ for NIR AF, and RS_{1320} and RS_{1660} for RS analysis) for the first cohort of 158 studied samples and 6-D space (additionally measured FI_{VIS} and $F\lambda_{VIS}$ for VIS AF) for the second cohort of 74 samples.

Figures 10 and 11 demonstrate 3-D representation of 4-D and 6-D space analysis, respectively. Complex optical methods show high efficiency of MM and BCC separation: the sensitivity and specificity of cancerous tissues classification are 94.9% and 92.5%, respectively, in 4-D criteria space, and 100% and 96.3% for 6-D criteria space.

The accuracy of MM and BCC separation is slightly higher for the six criteria algorithm. This fact may be caused both by increasing the data analyzed (additional VIS AF criteria) and by decreasing the number of the samples studied. A correlation between the chosen criteria was calculated in order to ensure the comparative increase of classification accuracy and its independence on the number of the tested tissue samples. Table 2 shows correlation matrixes for 6-D criteria space. Here, the bold font indicates the significant correlations (p value < 0.01).

4 Discussion and Conclusions

Let us compare the accuracy of different criteria and their combinations for cancerous tissue classification. The highest accuracy of MM and BCC separation by phase plane and linear DA was demonstrated with a combination of criteria FI_{NIR} and $F\lambda_{NIR}$, when one of the criteria showed that the neoplasm is melanoma. In this case, the values of the sensitivity and specificity for the diagnostics of MM were 100% and 63.0%, respectively. Total accuracy in this case is only 73.0% and it is even less than in the case of single $F\lambda_{NIR}$ criteria implementation. This result caused by a low specificity of criteria pair FI_{NIR}

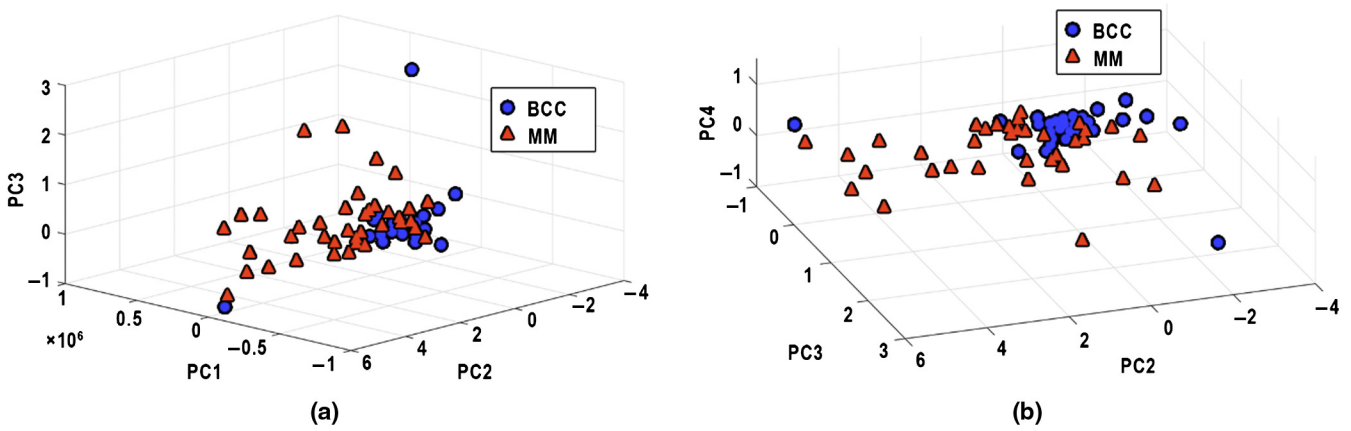

Fig. 10 MM and BCC classification with PCA in 4-D space (FI_{785}, $F\lambda_{785}$, RS_{1320}, and RS_{1660}): (a) PC1, PC2, and PC3 and (b) PC2, PC3, and PC4.

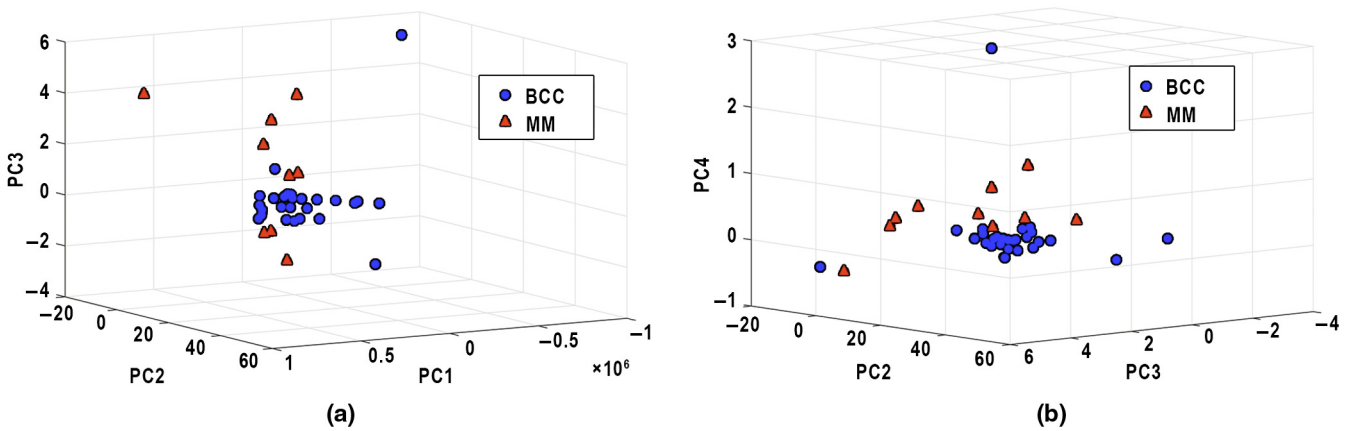

Fig. 11 MM and BCC classification with PCA in 6-D space (FI_{785}, $F\lambda_{785}$, RS_{1320}, RS_{1660}, FI_{457}, and $F\lambda_{457}$): (a) PC1, PC2 and PC3 and (b) PC2, PC3 and PC4.

Table 2 Correlation of criteria RS_{1320}, RS_{1660}, FI_{NIR}, $F\lambda_{NIR}$, FI_{VIS}, and $F\lambda_{VIS}$.

	RS_{1320}	RS_{1660}	FI_{NIR}	$F\lambda_{NIR}$	FI_{VIS}	$F\lambda_{VIS}$
RS_{1320}	**1.00**	**0.63**	**0.26**	**0.42**	**0.18**	0.12
RS_{1660}	**0.63**	**1.00**	0.02	**0.17**	0.08	**0.28**
FI_{NIR}	**0.26**	0.02	**1.00**	**0.25**	**0.32**	0.22
$F\lambda_{NIR}$	**0.42**	**0.17**	**0.25**	**1.00**	0.024	0.14
FI_{VIS}	**0.18**	0.08	**0.32**	0.024	**1.00**	0.08
$F\lambda_{VIS}$	0.12	**0.28**	0.22	0.14	0.08	**1.00**

Note: Significant correlations (p value < 0.01) are marked with bold font.

and $F\lambda_{NIR}$ as a sufficient number of BCC samples in this case are treated as MM samples. Detailed information about the accuracy of MM and BCC separation with different combinations of criteria is gathered in Table 3. Phase plane classification even with linear DA allows for MM and BCC classification with accuracy of 87%. This is possible with analysis of skin AF spectra simultaneously in NIR and visible regions. Analysis of AF spectra only in one of the spectral ranges shows 5% to 15% lower values of total accuracy of MM and BCC separation. The total accuracy of MM and BCC separation with different approaches varies from 50% to 97.3%. The lowest accuracy shows a combination of VIS AF and RS_{1660} criteria.

Table 3 Sensitivity and specificity of MM and BCC separation.

Criterions	Sensitivity (%)	Specificity (%)	Accuracy (%)
RS_{1320}	89.7	67.6	78.9
RS_{1660}	82.0	37.8	60.5
FI_{NIR}	74.4	47.5	60.8
$F\lambda_{NIR}$	69.2	85.0	77.2
FI_{VIS}	100	43.4	50.0
$F\lambda_{VIS}$	100	33.3	51.4
RS_{1320} and RS_{1660} (RS two-step method)	97.4	62.2	80.3
FI_{NIR} and $F\lambda_{NIR}$ (NIR AF)	92.3	37.5	64.6
FI_{VIS} and $F\lambda_{VIS}$ (VIS AF)	80.0	77.8	78.4
FI_{VIS} and $F\lambda_{NIR}$ (VIS and NIR AF)	70.0	92.6	86.5
FI_{NIR}, $F\lambda_{NIR}$, RS_{1320} and RS_{1660} (4-D criteria)	94.9	92.5	93.7
FI_{NIR}, $F\lambda_{NIR}$, RS_{1320}, RS_{1660}, FI_{VIS} and $F\lambda_{VIS}$ (6-D criteria)	100	96.3	97.3

These criteria show low related values of sensitivity and specificity, and overall accuracy of MM detection does not exceed 54%. The most useful criteria for MM and BCC separation appear to be RS_{1320} and $F\lambda_{NIR}$ showing an accuracy of 78.9% and 77.2%, respectively.

Comparison of achieved accuracy with other methods of MM diagnostics using AF techniques allows for drawing a conclusion about very similar results. For example, Borisova et al.[43] achieved accuracy of melanomas and nonmelanoma skin cancers separation equal to 93.6% due to a combination of AF and backscattered radiation analysis. Therefore, joint application of two spectroscopic techniques showed similar diagnostic accuracy of MM detection as the implementation of AF analysis in visible and NIR regions. The accuracy of 80% and 90% in AF skin cancer diagnosis in the NIR region was reported by Wang et al.[44] and that is comparable to the results shown in the current study. Significant improvement of AF diagnosis accuracy of skin tumors is possible with exogenous fluorophores monitoring.[45] However, implementation of exogenous fluorophores is expensive and requires their injection into a patient's body, which makes such AF study unacceptable for mass screening.

We may use more than two criteria to improve the accuracy of malignant tissue classification, as in this case, we estimate a wide set of tissues structural components alteration. Analysis of skin tissue classes with complex methods based on 4-D or 6-D criteria space shows the improvement in MM and BCC separation up to 8% to 11% in comparison with phase plane analysis, wherein accuracy of the 6-D algorithm is 3.6% higher than in the case of the 4-D algorithm. Such enhancement in accuracy is caused by better probability to find the highest differences between the chosen criteria in the multidimensional space. On the other hand, the data for 6-D criteria analysis were acquired for the fewer number of specimens and we have to estimate the correlation between criterions to understand their contribution in the classification accuracy.

The highest correlation coefficient achieved for a combination of diagnostic criteria is RS_{1320} and RS_{1660}, while criteria pair FI_{NIR} and RS_{1660} shows the lowest correlation (Table 2). Pairs of $F\lambda_{NIR}$, FI_{VIS}, and $F\lambda_{VIS}$ also show a rather low correlation in comparison with pairs FI_{NIR} and $F\lambda_{VIS}$, RS_{1320} and RS_{1660}. The correlation between RS_{1320} and RS_{1660} criteria may be explained by the acquired Raman spectra processing. Each Raman spectrum was normalized to the maximum, thus we observe the contribution of Raman band 1450 cm^{-1} in both RS_{1320} and RS_{1660} criteria. The presence of Raman band 1450 cm^{-1} leads to their strong correlation exceeding 0.6. The value of correlation between Raman criteria (RS_{1320} and RS_{1660}) and NIR AF criteria (FI_{NIR} and $F\lambda_{NIR}$) lies in the interval 0.02 to 0.43. Correlation value exceeding 0.4 may be explained by the impact of melanin in NIR AF and RS criteria. Huang et al.[46] showed that major melanin peaks lie in the bands 1380 and 1580 cm^{-1}. These peaks may be associated with bands CH_2, CH_3 and C=C. According to Huang et al.,[46] the concentration of melanin in the skin affects 1320 to 1340, 1450, and 1660 cm^{-1} bands. In turn, criteria FI_{NIR} and $F\lambda_{NIR}$ include information about melanin influence on AF spectra, and accordingly they are correlated with criteria RS_{1320} and RS_{1660}. This correlation plays the most significant role for criteria pair RS_{1320} and $F\lambda_{NIR}$, where it reaches the value of 0.43. It is reasonable to assume that such relatedly strong correlation is caused by the presence of MMs in studied samples, as melanomas contain a lot of melanin.

Correlation of visible AF criteria (FI_{VIS} and $F\lambda_{VIS}$) with RS criteria and NIR AF criteria does not exceed 0.28 and 0.32, correspondingly. This correlation is lower than the correlation between RS and NIR AF criteria and may be explained by different component compositions measured for VIS AF. One of the most important components measured for VIS AF is porphyrins. The content of porphyrins on the upper skin layers is determined by the presence of endogenous skin cells porphyrins and porphyrins produced by bacteria.[41] Stimulated spectra of skin and bacterial porphyrins contribute both in VIS AF and in currently studied RS bands, as porphyrins may contain a lot of CH_2, CH_3, C=N and C=C bands.[47] As a result, the presence of porphyrins influences the intensity of the chosen RS bands and thereby affects the criteria ratios RS_{1320} and RS_{1660}.

The lowest correlation shows criteria pairs FI_{VIS} and $F\lambda_{VIS}$ or FI_{VIS} and RS_{1660}. The correlation value is only 0.08 for both of those criteria pairs. Visible AF criteria utilize information from significantly different components. Criterion FI_{VIS} depends on the content of flavins and lipopigments, while criterion $F\lambda_{VIS}$ depends on tissue porphyrin content. In contrast, RS_{1660} criterion uses information from 1450 and 1660 cm^{-1} Raman bands, which are particularly caused by fatty acids[48] as lipid metabolism changes during the tumor growth.[49] Low correlation between criteria FI_{VIS} and RS_{1660} may be explained by the contribution of flavins in the FI_{VIS} criterion, since flavins have a rather small intensity in the 1660 cm^{-1} band.[50]

As some of the chosen criteria have strong correlations, we may reduce the number of criteria by selection of criteria with the lowest correlations in order to achieve maximum diagnostic accuracy in 3-D phase space. Figures 10 and 11 demonstrate 3-D projections of 4-D and 6-D phase spaces. In a 3-D space analysis, we use PCs with highest variations and with a lowest correlation between each other. This analysis provides accuracy

of 85% to 98% for MM and BCC separation. Differences in skin tissue separation accuracy for 4 and 6 criteria implementation are caused by additional VIS AF criteria. Those criteria have low correlation with Raman and NIR AF criterions, and their implementation increases the sensitivity and the specificity of MM and BCC separation by approximately 4%.

The accuracy of the skin cancerous tissue separation is almost 98% for complex multiparametric 6-D criteria. Thus, the proposed approach of MM and BCC classification may be successfully used in clinical applications. This accuracy is also high enough for screening applications, as sensitivity 100% of MM detection is achieved with specificity exceeding 90%. This conclusion is confirmed by the results of studies of Zhao et al.,[19] who demonstrate the applicability of RS for *in vivo* analysis of skin tissue malignancy with sensitivity 95% to 99% and specificity about 30% to 46%. But in contrast to our study, Zhao tried to classify malignant and nonmalignant tissues. The large review made by Pence and Mahadevan-Jansen[51] discusses different RS techniques of cancer diagnostics, including multimodal analysis with RS, AF, and backscattering applications. It was shown that sensitivity and specificity of malignant and nonmalignant tissue separation varied from 82% to 100% and from 72% to 100% correspondingly. On the other hand, combined NIR and VIS AF analysis with RS study increases the overall accuracy of MM and BCC separation by 17%; and this fact promises a chance to utilize the proposed multiparametric method in high-precision MM detection applications.

In general, multimodal optical classification of skin malignancies with system combining principles of RS, visible, and NIR AF shows high potential in MM and BCC diagnosis. The proposed approach may be implemented for *in vivo* clinical examinations by decreasing laser radiation doses to satisfy ANSI Standard for safe laser skin irradiation. This may be done by defocusing radiation up to spot size 3.5 mm with decreasing the lasers intensity on the skin below the value of 0.28 W/cm^2 or by decreasing of acquisition time up to 1 s using a more sensitive (or deeply cooled) detector, as in this case maximum permissible exposure will be limited to 1.55 W/cm^2.

Combination of AF analysis with RS study allows for increasing the joint sensitivity and specificity of MM detection up to 95% to 100% due to involvement in criteria analysis of the changes in concentration of porphyrins, flavins, and melanin along with RS criteria. High level of malignant skin tumors classification accuracy is indicative of high clinical potential of the proposed method. This method may be used both for precise tumor type determination and for mass screening surveys. For example, fast analysis of large tissue areas may be performed on the first step only with NIR and VIS AF criteria, as the AF signal is much more intense than an RS signal and may be collected during a short time. The accuracy of only AF skin tissue analysis is about 87% and it may be increased by RS analysis of the suspicious areas on the next step. Such joint analysis will be characterized by 100% sensitivity with 96% specificity.

We have demonstrated that the proposed multiparametric complex RS and AF analysis is rapid, reliable, and cost effective as it may be done simultaneously and in a single device. Moreover, further enhancement of diagnostics effectiveness may be achieved by including imaging modalities. For example, Wang et al.[52] showed a possibility to combine RS and OCT for tissue malignancy study. Another possible area of complex RS and AF method implementation is hyperspectral imaging[53] with simultaneous registration of spectral data cube for both tumors and healthy skin. As a result, hyperspectral imaging may most effectively utilize the proposed 6-D criteria method.

Disclosures

All authors declare no conflict of interests for this paper and have no financial interest in the materials used in the paper.

Acknowledgments

This research was supported by the Ministry of Education and Science of the Russian Federation.

References

1. P. E. Goss et al., "Challenges to effective cancer control in China, India, and Russia," *Lancet Oncol.* **15**, 489–538 (2014).
2. M. I. Davydov and E. M. Axel, *Statistics of Malignancies in Russia and the CIS Countries in 2012*, Bulletin of ROSC, Moscow (2014).
3. M. Ulricha, S. Lange-Asschenfeldt, and S. González, "In vivo reflectance confocal microscopy for early diagnosis of nonmelanoma skin cancer," *Actas Dermosifiliogr.* **103**(9), 784–789 (2012).
4. M. Mogensen et al., "OCT imaging of skin cancer and other dermatological diseases," *J. Biophoton.* **2**(6–7), 442–451 (2009).
5. K. Koenig, "Hybrid multiphoton multimodal tomography of in vivo human skin," *IntraVital.* **1**(1), 11–26 (2014).
6. S. Seidenari et al., "Multiphoton laser tomography and fluorescence lifetime imaging of melanoma morphologic features and quantitative data for sensitive and specific non-invasive diagnostics," *PLoS One.* **8**(7), e70682 (2013).
7. S. Seidenari et al., "Multiphoton laser microscopy and fluorescence lifetime imaging for the evaluation of the skin," *Dermatol. Res. Pract.* **2012**, 810749 (2012).
8. A. Forsea et al., "Clinical application of optical coherence tomography for the imaging of non-melanocytic cutaneous tumors: a pilot multimodal study," *J. Med. Life.* **3**(4), 381–389 (2010).
9. W. Gao et al., "Medical images classification for skin cancer using quantitative image features with optical coherence tomography," *J. Innov. Opt. Health Sci.* **9**(4), 1650003 (2016).
10. D. S. Raupov et al., "Skin cancer texture analysis of OCT images based on Haralick, fractal dimension and the complex directional field features," *Proc. SPIE* **9887**, 98873F (2016).
11. R. Wessels et al., "Optical biopsy of epithelial cancers by optical coherence tomography (OCT)," *Lasers Med. Sci.* **29**(3), 1297–1305 (2014).
12. T. Upile et al., "A new tool to inform intra-operative decision making in skin cancer treatment: the non-invasive assessment of basal cell carcinoma of the skin using elastic scattering spectroscopy," *Head Neck Oncol.* **4**(3), 74 (2012).
13. H. Lui et al., "Real-time Raman spectroscopy for in vivo skin cancer diagnosis," *Cancer Res.* **72**(10), 2491–2500 (2012).
14. E. Borisova et al., "Diagnostics of pigmented skin tumors based on laser-induced autofluorescence and diffuse reflectance spectroscopy," *Quantum Electron.* **38**, 597–605 (2008).
15. Y. Pu et al., "Stokes shift spectroscopic analysis of multifluorophores for human cancer detection in breast and prostate tissues," *J. Biomed. Opt.* **18**(1), 017005 (2013).
16. M. S. Bergholt et al., "Raman endoscopy for objective diagnosis of early cancer in the gastrointestinal system," *J. Gastroint. Dig. Syst.* **S1**, 008 (2013).
17. S. Wachsmann-Hogiu, T. Weeks, and T. Huser, "Chemical analysis in vivo and in vitro by Raman spectroscopy—from single cells to humans," *Curr. Opin. Biotechnol.* **20**(1), 63–73 (2009).
18. W. Liu et al., "Dual laser-induced fluorescence: progress and perspective for in vivo cancer diagnosis," *Chin. Sci. Bullet.* **58**(17), 2003–2016 (2013).
19. J. Zhao et al., "Real-time Raman spectroscopy for automatic in vivo skin cancer detection: an independent validation," *Anal. Bioanal. Chem.* **407**, 8373–8379 (2015).
20. L. Marcu, "Fluorescence lifetime techniques in medical applications," *Ann. Biomed. Eng.* **40**(2), 304–331 (2012).

21. M. S. Bergholt et al., "Combining near-infrared-excited autofluorescence and Raman spectroscopy improves *in vivo* diagnosis of gastric cancer," *Biosens. Bioelectron.* **26**(10), 4104–4110 (2011).
22. M. A. Short et al., "Using laser Raman spectroscopy to reduce false positives of autofluorescence bronchoscopies," *J. Thorac. Oncol.* **6**(7), 1206–1214 (2011).
23. X. Li and D. Wang, "Spectral analysis of lung cancer serum using fluorescence and Raman spectroscopy," *Proc. SPIE* **6088**, 608809 (2006).
24. X. Li et al., "Study of method and system for diagnosis of cancer using autofluorescence and Raman spectroscopy," *International Conference on Engineering in Medicine and Biology Society*, Vol. 5, pp. 5453–5436, IEEE (2005).
25. S. Jeong et al., "Fluorescence-Raman dual modal endoscopic system for multiplexed molecular diagnostics," *Sci. Rep.* **5**, 9455 (2015).
26. V. P. Zakharov et al., "Comparative analysis of combined spectral and optical tomography methods for detection of skin and lung cancers," *J. Biomed. Opt.* **20**(2), 025003 (2015).
27. M. E. Darvin, N. N. Brandt, and J. Lademann, "Photobleaching as a method of increasing the accuracy in measuring carotenoid concentration in human skin by Raman spectroscopy," *Opt. Spectrosc.* **109**(2), 205–210 (2010).
28. H. Wang et al., "Improving skin Raman spectral quality by fluorescence photobleaching," *Photodiagn. Photodyn. Ther.* **9**, 299–302 (2012).
29. J. Zhao et al., "Automated autofluorescence background subtraction algorithm for biomedical Raman spectroscopy," *Soc. Appl. Spectrosc.* **61**(11), 1225–1232 (2007).
30. E. B. Hanlon et al., "Prospects for in vivo Raman spectroscopy," *Phys. Med. Biol.* **45**, R1–R59 (2000).
31. K. E. Shafer-Peltier et al., "Raman microspectroscopic model of human breast tissue: implications for breast cancer diagnosis in vivo," *J. Raman Spectrosc.* **33**, 552–563 (2002).
32. R. O. Duda, P. E. Hart, and D. G. Stork, *Pattern Classification*, 2nd ed., Wiley (2001).
33. J. A. Nelder and R. Mead, "A simple method for function minimization," *Comput. J.* **7**, 308–313 (1965).
34. Y. A. Khristoforova et al., "Method of autofluorescence diagnostics of skin neoplasms in the near infrared region," *J. Biomed. Photonics Eng.* **1**(3), 186–192 (2015).
35. I. A. Bratchenko et al., "Malignant melanoma and basal cell carcinoma detection with 457 nm laser-induced fluorescence," *J. Biomed. Photonics Eng.* **1**(3), 180–185 (2015).
36. B. Barton and J. Peat, *Medical Statistics: A Guide to SPSS, Data Analysis and Critical Appraisal*, 2nd ed., John Wiley & Sons, New York (2014).
37. M. Ringnér, "What is principal component analysis?" *Nat. Biotechnol.* **26**, 303–304 (2008).
38. L. Feller et al., "Basal cell carcinoma, squamous cell carcinoma and melanoma of the head and face," *Head Face Med.* **12**(11), (2016).
39. A. Pappas, "Epidermal surface lipids," *Dermato-Endocrinol.* **1**(2), 72–76 (2014).
40. I. Seo et al., "Fluorescence spectroscopy for endogenous porphyrins in human facial skin," *Proc. SPIE* **7161**, 716103 (2009).
41. M. Shu et al., "Porphyrin metabolisms in human skin commensal propionibacterium acnes bacteria: potential application to monitor human radiation risk," *Curr. Med. Chem.* **20**(4), 562–568 (2013).
42. D. L. Fox, *Biochromy, Natural Coloration of Living Things*, University of California Press, Berkeley (1979).
43. E. Borisova et al., "Light-induced autofluorescence and diffuse reflectance spectroscopy in clinical diagnosis of skin cancer," *Proc. SPIE* **9129**, 91291O (2014).
44. S. Wang et al., "In vivo near-infrared autofluorescence imaging of pigmented skin lesions: methods, technical improvements and preliminary clinical results," *Skin Res. Technol.* **19**, 20–26 (2013).
45. E. G. Borisova, L. P. Angelova, and E. P. Pavlova, "Endogenous and exogenous fluorescence skin cancer diagnostics for clinical applications," *IEEE J. Sel. Top. Quantum Electron.* **20**(2), 7100412 (2014).
46. Z. Huang et al., "Raman spectroscopy of in vivo cutaneous melanin," *J. Biomed. Opt.* **9**(6), 1198–1205 (2004).
47. K. S. Suslick et al., "The materials chemistry of porphyrins and metalloporphyrins," *J. Porphyrins Phthalocyanines* **4**, 407–413 (2000).
48. K. Czamara et al., "Raman spectroscopy of lipids: a review," *J. Raman Spectrosc.* **46**(1), 4–20 (2015).
49. E. Currie et al., "Cellular fatty acid metabolism and cancer," *Cell Metab.* **18**(2), 153–161, (2013).
50. M. D. Altose et al., "Comparing protein–ligand interactions in solution and single crystals by Raman spectroscopy," *Proc. Natl. Acad. Sci. U. S. A.* **98**(6), 3006–3011 (2001).
51. I. Pence and A. Mahadevan-Jansen, "Clinical instrumentation and applications of Raman spectroscopy," *Chem. Soc. Rev.* **45**(7), 1958–1979 (2016).
52. J. Wang et al., "Development of a hybrid Raman spectroscopy and optical coherence tomography technique for real-time in vivo tissue measurements," *Opt. Lett.* **41**(13) 3045–3048 (2016).
53. G. Lua and B. Fei, "Medical hyperspectral imaging: a review," *J. Biomed. Opt.* **19**(1), 010901 (2014).

Ivan A. Bratchenko graduated from Samara State Aerospace University (SSAU) in 2009 and received his PhD in 2011 from the same university. At the moment, he is an associate professor in the Laser and Biotechnical Systems Department, Samara University, and a leading researcher at Photonics Laboratory. His main projects at Photonics Laboratory are associated with spectroscopic applications for analysis of tissues and biofluids in medical applications, including *in vivo* and *ex vivo* detection of neoplasms with hyperspectral imaging, Raman and fluorescent spectroscopy. His research interests include optics, biophotonics, spectroscopy, mathematical modeling of light propagation in tissues, hyperspectral imaging, optical coherence tomography (OCT), and lab-on-a-chip technologies.

Dmitry N. Artemyev is a postgraduate student at the Laser and Biotechnical Systems Department, Samara University. He graduated from the Faculty of Information Science, Samara University, in 2013. He has a master's degree in applied mathematics and physics. His research interests include spectroscopy, Raman spectroscopy (RS), autofluorescence, optical methods for diagnosis, biophotonics, and lab-on-a-chip technologies.

Oleg O. Myakinin received his bachelor's and master's degrees in applied mathematics and computer science at SSAU in 2009 and 2011, respectively. Now, he is a postgraduate student at Samara University (ex-SSAU) with Technical Cybernetics Department as well as research scientist at Lasers and Biotechnical Systems Department. His research interests include computer vision, OCT, and biomedical image processing.

Yulia A. Khristoforova is a postgraduate student at the Laser and Biotechnical Systems Department, Samara University. She received her bachelor's and master's degree in applied mathematics and physics from SSAU in 2013 and 2015, respectively. Her research interests include biophotonics, RS, and fluorescence spectroscopy.

Alexander A. Moryatov is an oncologist at the Endoscopy Department, Samara Regional Clinical Oncology Dispensary. He received his MD from Samara State Medical University in 2007. Since 2012, he has been an associate professor in the Samara State Medical University Oncology Department. His research interests include minimally invasive surgery, endosonography, photodynamic therapy, radiofrequency ablation, and skin and lung cancers.

Sergey V. Kozlov is the Honored Doctor of Russian Federation and currently head of the Oncology Department, Samara State Medical University. He received his MD in 1989 and DSc in medicine in 2001 from Samara State Medical University. His research interests include breast cancer, endosonography, photodynamic therapy, radiofrequency ablation, and skin lesions detection and treatment.

Valery P. Zakharov received his PhD in theoretical physics from Bogolyubov Institute for Theoretical Physics, Kiev, Ukraine, in 1984 and his DSc degree in optics from SSAU (now Samara University) in 1999. Currently, he is a professor and holds the Laser and Biotechnical Systems Chair. He is also a head of Photonics Research Laboratory, Samara University. His research interests include biophotonics, biomedical optics, spectroscopy, laser physics and techniques, plasma physics, and medical lasers.